

Effect of graphene grain boundaries on MoS_2/graphene heterostructures

Yue Zhang(张悦), Xiangzhe Zhang(张祥喆), Chuyun Deng(邓楚芸), Qi Ge(葛奇), Junjie Huang(黄俊杰), Jie Lu(卢捷), Gaoxiang Lin(林高翔), Zekai Weng(翁泽锴), Xueao Zhang(张学骜), Weiwei Cai(蔡伟伟)

Citation: Chin. Phys. B . 2020, 29(6): 067403 . **doi:** 10.1088/1674-1056/ab8a37
Journal homepage: http://cpb.iphy.ac.cn; http://iopscience.iop.org/cpb

What follows is a list of articles you may be interested in

Application of graphene vertical field effect to regulation of organic light-emitting transistors

Hang Song(宋航), Hao Wu(吴昊), Hai-Yang Lu(陆海阳), Zhi-Hao Yang(杨志浩), Long Ba(巴龙)

Chin. Phys. B . 2020, 29(5): 057401 . **doi:** 10.1088/1674-1056/ab81f3

Visible-to-near-infrared photodetector based on graphene-$MoTe_2$-graphene heterostructure

Rui-Xue Hu(户瑞雪), Xin-Li Ma(马新莉), Chun-Ha An(安春华), Jing Liu(刘晶)

Chin. Phys. B . 2019, 28(11): 117802 . **doi:** 10.1088/1674-1056/ab4576

Efficient doping modulation of monolayer WS_2 for optoelectronic applications

Xinli Ma(马新莉), Rongjie Zhang(张荣杰), Chunhua An(安春华), Sen Wu(吴森), Xiaodong Hu(胡晓东), Jing Liu(刘晶)

Chin. Phys. B . 2019, 28(3): 037803 . **doi:** 10.1088/1674-1056/28/3/037803

Influences on oxidation voltage and holding time on poly(3-methylthiophene) film for electrochromic stability

Bo Zhang(张波), Chen Xu(徐晨), Guo-Yue Xu(徐国跃), Chu-Yang Liu(刘初阳), Hong-Han Bu(卜红寒), Jian-Chao Zhang(张建超)

Chin. Phys. B . 2018, 27(12): 127802 . **doi:** 10.1088/1674-1056/27/12/127802

Optical spectroscopy studies on $FeTe_{1-x}Se_x$ and $A_xFe_{2-y}Se_2$ (A=K, Rb, Cs)：A brief overview

Yuan Rui-Hua, Wang Nan-Lin

Chin. Phys. B . 2013, 22(8): 087404 . **doi:** 10.1088/1674-1056/22/8/087404

SPECIAL TOPIC — Topological 2D materials

Effect of graphene grain boundaries on MoS_2/graphene heterostructures*

Yue Zhang(张悦)[1], Xiangzhe Zhang(张祥喆)[2], Chuyun Deng(邓楚芸)[2], Qi Ge(葛奇)[3], Junjie Huang(黄俊杰)[1], Jie Lu(卢捷)[1], Gaoxiang Lin(林高翔)[1], Zekai Weng(翁泽锴)[1], Xueao Zhang(张学骜)[1,3,†] and Weiwei Cai(蔡伟伟)[1,3,‡]

[1] *College of Physical Science and Technology, Xiamen University, Xiamen* 361005, *China*
[2] *College of Arts and Science, National University of Defense Technology, Changsha* 410073, *China*
[3] *Chongqing 2D Materials Institute, Chongqing* 400714, *China*

(Received 15 December 2019; revised manuscript received 13 April 2020; accepted manuscript online 16 April 2020)

The grain boundaries of graphene are disordered topological defects, which would strongly affect the physical and chemical properties of graphene. In this paper, the spectral characteristics and photoresponse of MoS_2/graphene heterostructures are studied. It is found that the blueshift of the G and 2D peaks of graphene in Raman spectrum is due to doping. The lattice mismatch at the graphene boundaries results in a blueshift of MoS_2 features in the photoluminescence spectra, comparing to the MoS_2 grown on SiO_2. In addition, the photocurrent signal in MoS_2/hexagonal single-crystal graphene heterostructures is successfully captured without bias, but not in MoS_2/polycrystalline graphene heterostructures. The electron scattering at graphene grain boundaries affects the optical response of MoS_2/graphene heterostructures. The photoresponse of the device is attributed to the optical absorption and response of MoS_2 and the high carrier mobility of graphene. These findings offer a new approach to develop optoelectronic devices based on two-dimensional material heterostructures.

Keywords: photoresponse, heterostructures, grain-boundary

PACS: 74.25.Gz, 78.20.Jq, 42.70.Gi **DOI:** 10.1088/1674-1056/ab8a37

1. Introduction

The discovery of graphene has opened the door to study other two-dimensional (2D) materials,[1–5] such as 2D metal chalcogenides (2DMCs), black phosphorus, and so on.[6] These materials have attracted great interest owing to their completely different electronic structures from those of bulk materials. Furthermore, novel electronic properties and photoresponse can be achieved, due to the integration of two or more 2D materials.[7,8] On account of its atomic-level thickness, the layered heterostructure also provides excellent optical transparency and good mechanical flexibility.[9]

Graphene is expected to be used in many electronic devices due to its high conductivity and high carrier mobility. However, its low photoresponse limits its potential.[10–12] Single layer MoS_2 has high optical absorption and distinct photoluminescence (PL). Nonetheless, it has low carrier mobility, which affects its responsivity. Therefore, the two materials can complement each other in the MoS_2/graphene heterostructures. The single layer MoS_2 can enhance the optical absorption, while transfer photo-generated carriers effectively to graphene.[13] New photoelectric devices have been developed based on these heterostructures, such as high gain photodetectors and optical responding memories.[14] MoS_2 is used as the sensitizer of light, and graphene with high mobility is used as highway to transport the photo-excited carrier. In this case, the combination of high optical absorption and fast electron transportation makes the MoS_2/graphene phototransistors more responsive (up to 10^8 A/W) than those with only graphene or MoS_2.[15,16]

Nonetheless, the existence of grain boundaries (GBs) leads to the deterioration of physical properties of graphene, such as the decrease of chemical reactivity,[17] thermal conductivity,[18] and carrier mobility.[19] This, means that growing single-crystal graphene (SCG), identifying and modifying its GBs are very important for practical applications. The GBs of graphene are disordered topological defects, which strongly affect the physical and chemical properties of graphene,[20] therefore, its application in devices. Recent research shows that the distribution of defects at grain boundaries is linear periodic.[21] In general, nonhexagonal rings (such as five-, seven-, and eight-membered rings) exist at the grain boundaries to mediate the lattice mismatch between two graphene domains.[22] The inherent topological defects can accommodate lattice defects, but retain three folds of sp^2 bonding of carbon atoms.[21] Topological defects are also the basis of polycrystalline graphene. Such defects may adversely affect the thermal and electronic properties of graphene, such as reducing the electronic mobility. The growth of MoS_2 on

*Project supported by the National Natural Science Foundation of China (Grant No. 11874423).
†Corresponding author. E-mail: xazhang@xmu.edu.cn
‡Corresponding author. E-mail: wwcai@xmu.edu.cn
© 2020 Chinese Physical Society and IOP Publishing Ltd

graphene depends on van der Waals interaction, which can be used to mark the graphene GBs.[23] Therefore, it is crucial to investigate the influence of graphene GBs on the photoelectric response of MoS_2/graphene heterostructures.

In this paper, single crystal MoS_2 is deposited on hexagonal single-crystal graphene (HSCG) by molecular beam epitaxy (MBE). There is only one orientation of MoS_2 on SCG. The spectral characteristics and photoresponse of the samples are measured. The G and 2D peaks of graphene demonstrate a blueshift after growing a monolayer of MoS_2. The quenching of PL of MoS_2 is remarkable, while the PL peaks at the MoS_2/graphene GBs shift toward short wavelength. Besides, the photocurrent signal in the MoS_2/HSCG heterostructures is successfully measured without bias.

2. Experimental details

The HSCGs were grown by inserting transition metal into Cu pocket.[24,25] SLG was grown on the Cu pocket via the low-pressure-chemical-vapor-deposition process.[23] After that, the polymethyl methacrylate (PMMA)-assisted method was used to transfer the graphene onto SiO_2/Si substrates[26] for further synthesis. MoS_2 crystals were grown by an MBE system using MoO_3 and S powder as precursors.[23] The aqueous solution (2 M NaOH) at 90 ℃ was used to transfer the MoS_2/graphene onto Cu grids. Finally, electron beam lithography was used to prepare a pair of Ti/Au electrodes.[27]

The surface morphology of materials was characterized by a scanning electron microscope (SEM) (Zeiss Sigma). A Raman spectrometer (Alpha 300, WITec) with a 488 nm laser excitation source was used to measure Raman and PL spectra. The photocurrent was measured using the Raman spectrometer with a 532 nm laser. TEM (JEM-2100, operated at 200 keV with a point-to-point resolution of 0.19 nm) was used to probe the heterostructures jointly with selected area electron diffraction (SAED) patterns.

3. Results and discussion

A few number of HSCG domains on Cu pocket are observed by SEM, as shown in Fig. 1(a). Besides, the sizes of the HSCG domains are about 40–60 μm. An SLG membrane up to 5 cm (Fig. 1(b)) was also prepared. It is a common method to transfer the grown graphene onto target substrates using poly(methyl methacrylate) PMMA.[26] Then the MoS_2 single crystals were synthesized on the graphene/SiO_2/Si substrates using the MBE method. After that, a hot alkali etching method was used to transfer the samples onto Cu grids.[23,28] There is only one orientation for MoS_2 grown on HSCG (Fig. 1(c)), while various orientations of MoS_2 are observed when deposited on polycrystalline graphene. Therefore, the location and the size of graphene grain boundaries can be identified in this way easily, as shown in Fig. 1(d).

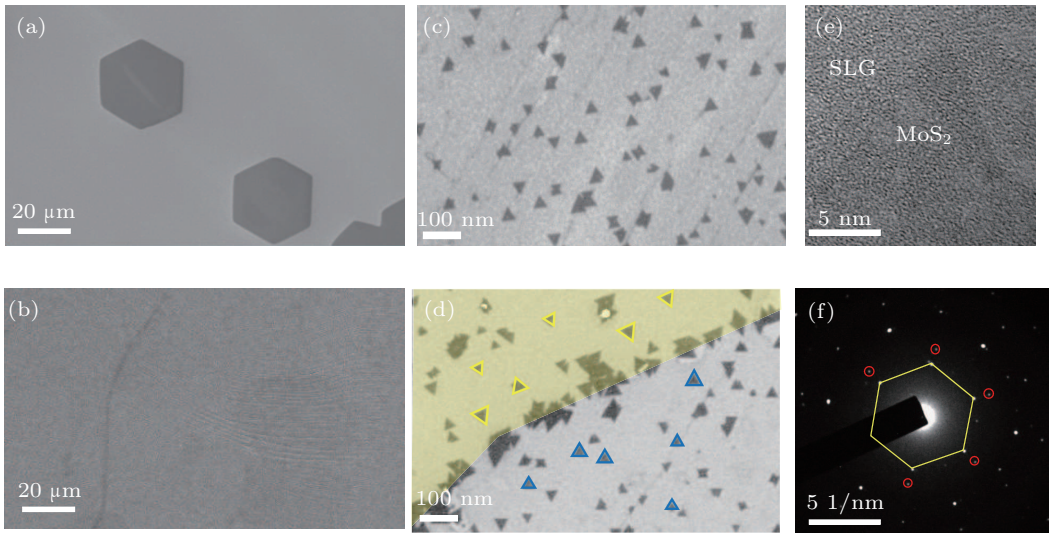


Fig. 1. SEM image of (a) hexagonal single-crystal graphene and (b) single layer graphene membrane grown on cooper foil. (c) Enlarged SEM image of single crystal MoS_2 grown on HSCG domain. (d) Enlarged SEM image of MoS_2/SLG GBs heterostructures. (e) TEM image of MoS_2. (f) SAED pattern of (e).

To confirm the orientation of the MoS_2/graphene heterostructures, high resolution TEM (HR-TEM) images of the heterostructures and corresponding diffraction patterns were obtained by using TEM and SAED. Figure 1(e) shows a triangular MoS_2 single crystal on the graphene film, whose edges can be exhaustively scrutinized. The SAED clearly shows two sets of hexagonal patterns from MoS_2 and graphene without any deviation from the lattice orientation, which suggests that the MoS_2 single crystals are grown epitaxially on the graphene substrates through van der Waals (Fig. 1(f)).

Figure 2(a) displays an SEM image of the MoS_2/HSCG heterostructures. The Raman spectra of the graphene show several differences before and after the growth of MoS_2, as shown in Fig. 2(b). Before MoS_2 deposition, the characteris-

tic G and 2D peaks of graphene are observed, while the D band which represents defects in graphene is absent. The intensity ratio of 2D/G band is almost 2 : 1, confirming the growth of high quality SLG.[29,30] After MoS_2 deposition, a broad background of PL from MoS_2 is observed, confirming that both the graphene and MoS_2 are present. Furthermore, the intensity of the 2D peak is reduced, but a D peak with weak intensity emerges. Note, the G and 2D peaks also show a blueshift. This indicates that the growth of MoS_2 slightly influences the quality of graphene.

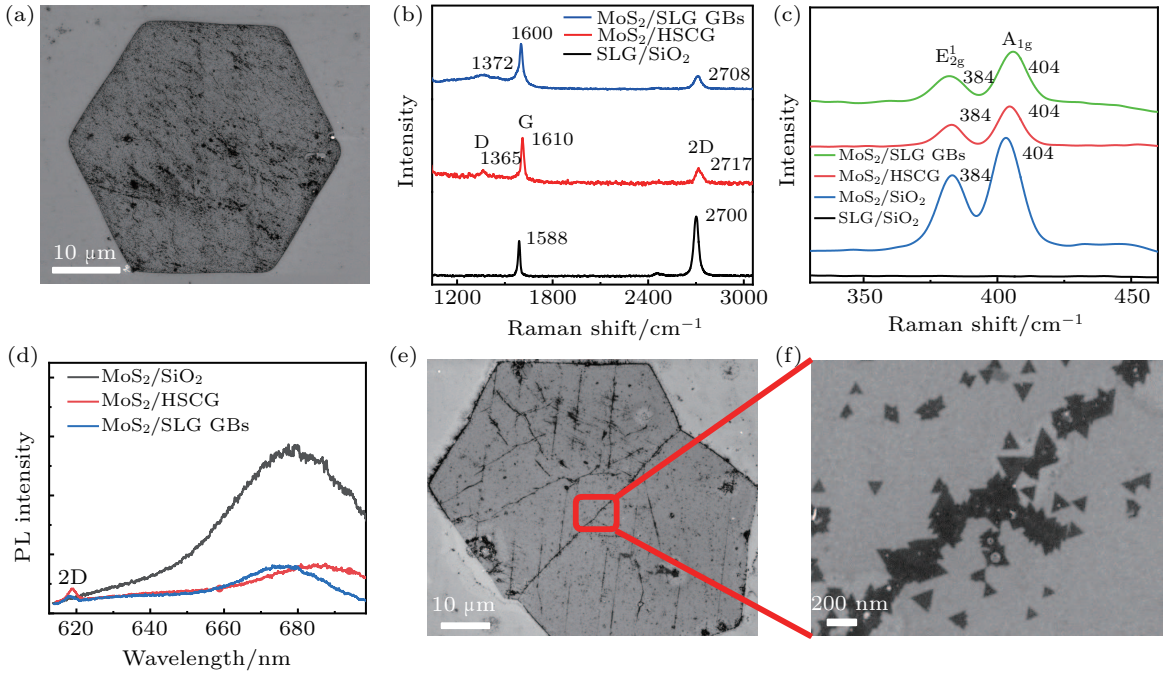


Fig. 2. (a), (e) SEM images of MoS_2/graphene heterostructures. (b) Raman spectrum of the SLG and heterostructures. (c) Raman spectrum of the MoS_2 and heterostructures. (d) PL spectrum of MoS_2 on SLG and SiO_2. (f) Enlarged SEM image corresponding to the red rectangle in (e).

It is known that elevated temperature, charge transfer, and strain affect the position of the 2D peak of graphene. Since the spectrum is measured at room temperature, the blueshifts of the G and 2D peaks are not due to increasing temperature. On the other hand, the van der Waals contact between graphene and MoS_2 tends to change the doping level,[31] while the increase of the doping concentration generally leads to a reduction of the I_{2D}/I_G ratio.[5] Therefore, the blueshift in this case may due to doping.

The Raman spectra with characteristic MoS_2 features are measured and shown in Fig. 2(c). The A_{1g} and E^1_{2g} peaks are located at 404 cm^{-1} and 384 cm^{-1} respectively. It confirms the growth of the single layer of MoS_2.[32–34] Unsurprisingly, no MoS_2 related peaks are observed in the graphene samples. The Raman spectra for MoS_2 domains grown on SiO_2 are also investigated for comparison. The A_{1g} and E^1_{2g} peaks for MoS_2 on SiO_2 show a higher intensity compared with those on graphene. It is known that single layer MoS_2 has a strong PL.[11] The PL spectra of MoS_2 grown on HSCG, graphene GBs, and SiO_2 are shown in Fig. 2(d). The intensity of PL is strongly suppressed for the heterostructures. It is clear that the PL of the MoS_2 grown on graphene is strongly quenched, which proves the existence of electronic interaction between graphene and MoS_2. Interestingly, the characteristic PL features of MoS_2 grown on graphene GBs show a blueshift, which may result from the lattice mismatch. It can be seen from Fig. 2(f) that MoS_2 grows more densely on the graphene GBs, without the typical triangle shape. This may be the reason for the blueshift of the PL. MoS_2 domains directly grown on graphene show stronger interaction with graphene, which is crucial for effective interlayer coupling.

Figures 3(a) and 3(b) show the Raman mapping of graphene grown by CVD method. These two figures prove that the graphene grown by inserting Mo sheet into copper pocket has high quality. Figures 3(c) and 3(d) show the G and 2D peaks of graphene after MoS_2 growth by MBE, respectively. There are defects on the surface of graphene after MoS_2 growth since the 2D band intensity decreases. Based on the mapping of MoS_2 A_{1g} and E^1_{2g} bands (Figs. 3(e) and 3(f)), MoS_2 tends to grow at graphene GBs and folding. Figure 3(g) is the MoS_2/HSCG PL mapping which shows that the PL distribution on the graphene surface is relatively uniform. This makes the subsequent measurement of photocurrent feasible.

The photocurrent signal is successfully captured by irradiation of a 532 nm laser without bias, which proves the presence of photoinduced electron transfer from MoS_2 to graphene. Figure 4(a) is a schematic diagram of the device and figure 4(b) is the optical micrograph of the MoS_2/HSCG

heterostructure. Raman intensity mapping of the G band of graphene shown in Fig. 4(e) confirms the growth of high quality graphene. Therefore, the photocurrent signal is not likely caused by breakage of graphene. The boundaries between graphene and SiO_2 can be seen clearly in the mapping of photocurrent of the device, as shown in Fig. 4(c).

The photocurrent near the MoS_2/graphene interface in Fig. 4(c) originates from the interaction of photogating, hot carriers, and other factor. The different position and strength of the metal at the upper and lower ends of the picture prove that the device has formed a path in the circuit. Meanwhile, the photocurrent was also measured at the place where metal–graphene contacted. This is because the potential barriers and built-in electric field might emerge at the electrode/graphene and MoS_2/graphene interfaces due to change of Fermi level of adjacent graphene.[13]

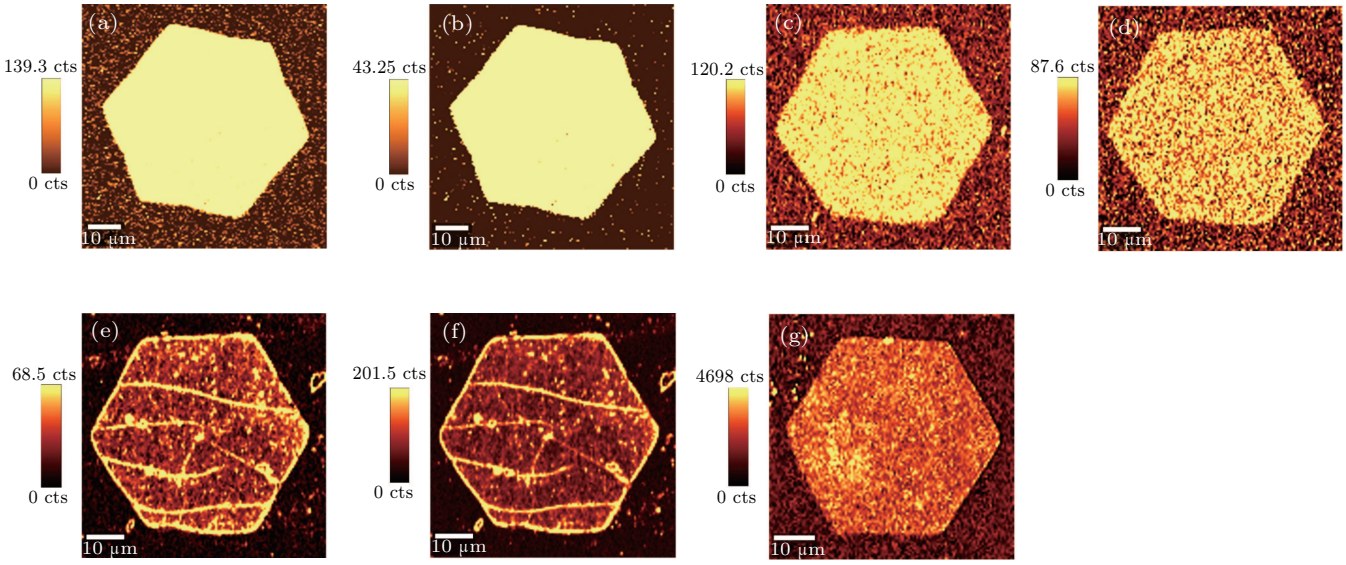


Fig. 3. Raman mapping images of the G peak (a) and 2D peak (b) of graphene, G peak (c) and 2D peak (d) of the graphene after MoS_2 growth. (e), (f) Raman mapping images of A_{1g} and E^1_{2g} bands of the MoS_2 grown on HSCG. (g) PL mapping of the MoS_2 grown on HSCG.

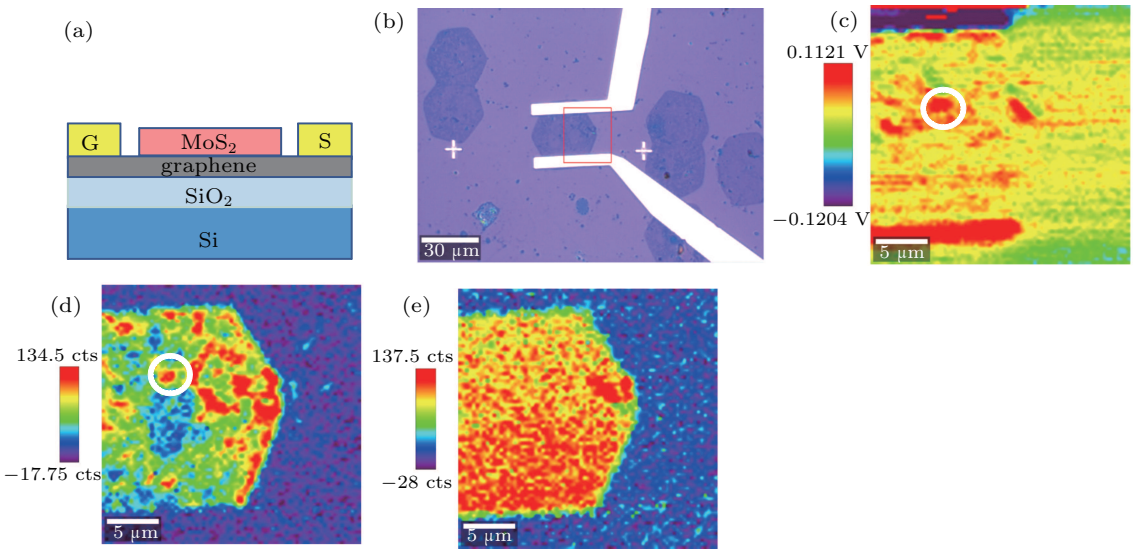


Fig. 4. (a) Schematic of MoS_2/HSCG heterostructure device. (b) Optical micrograph of the MoS_2/HSCG heterostructure and corresponding (c) Raman photocurrent mapping and (d) the A_{1g} band of MoS_2. (e) Raman intensity mapping of the G band of graphene.

The photothermoelectric effect (PTE) will form a photogenerated voltage V_{PTE} and generate a photocurrent in graphene,[35,36] due to the interaction between electrons. The photoresponse can be calculated by $V_{PTE} = (S_2 - S_1)\Delta T$, where S_1 and S_2 are the Seebeck coefficients, and ΔT is the temperature difference. Therefore, the photothermoelectric effect is one of the causes of the photocurrent in this case.

As shown in Fig. 4(d), the distribution of MoS_2 is not uniform. Note the intensity is positively correlated with the density of MoS_2. By comparing Figs. 4(c) and 4(d), the photocurrent signal captured in the white circle corresponds to the intensity of the A_{1g} band of MoS_2, which proves that the photocurrent is due to the presence of MoS_2. However, it is worth mentioning that figures 4(c) and 4(d) do not correspond to

each other exactly, which may be caused by the following reasons. The size of MoS_2 is at nm level, which is smaller than the spatial resolution of Raman mapping, which also affects the interpretation of the experimental results. If the MoS_2 is too small or the density is low, the photocurrent is hard to detect. Therefore, the spatial resolutions of Raman intensity and photocurrent are not perfectly identical. In contrast, no photocurrent is observed on MoS_2/SLG membrane heterostructures, which may be due to the topological defects of the polycrystalline grain boundaries. The topological defects affect the transmission of electrons and reduce the electrical properties of graphene, which eventually affects the collection of photocurrent.

4. Conclusions

In summary, the MoS_2/graphene heterostructures are prepared and the spectra and photoresponse are systematically investigated. It is observed that MoS_2 can mark the position of graphene grain boundaries, and the PL of MoS_2 is quenched after growing on graphene. The PL peak position of MoS_2 grown on graphene grain boundaries shows a blueshift due to the lattice mismatch. Besides, the photocurrent signal is observed in MoS_2/hexagonal single-crystal graphene heterostructures without a bias, but not in MoS_2/ polycrystalline graphene heterostructures. The electron scattering at the graphene grain boundaries affects the optical response of MoS_2/graphene heterostructures. The effect of graphene GBs on MoS_2/graphene heterostructures may have wide applications in optoelectronics devices.

References

[1] Wang Q H, Kalantar-Zadeh K, Kis A, Coleman J N and Strano M S 2012 *Nat. Nanotechnol.* **7** 699

[2] Butler S Z, Hollen S M, Cao L, Cui Y, Gupta J A, Gutierrez H R, Heinz T F, Hong S S, Huang J, Ismach A F, Johnston-Halperin E, Kuno M, Plashnitsa V V, Robinson R D, Ruoff R S, Salahuddin S, Shan J, Shi L, Spencer M G, Terrones M, Windl W and Goldberger J E 2013 *ACS Nano* **7** 2898

[3] Chhowalla M, Shin H S, Eda G, Li L J, Loh K P and Zhang H 2013 *Nat. Chem.* **5** 263

[4] Xu M, Liang T, Shi M and Chen H 2013 *Chem. Rev.* **113** 3766

[5] Ago H, Endo H, Solis-Fernandez P, Takizawa R, Ohta Y, Fujita Y, Yamamoto K and Tsuji M 2015 *ACS Appl. Mater. Interfaces* **7** 5265

[6] Wang C C, Liu X S, Wang Z Y, Zhao M, He H and Zou J Y 2018 *Chin. Phys. B* **27** 118106

[7] Lim H, Yoon S I, Kim G, Jang A R and Shin H S 2014 *Chem. Mater.* **26** 4891

[8] Hu R X , Ma X L , An C H and Liu J 2019 *Chin. Phys. B* **28** 117802

[9] Lee G H, Yu Y J, Cui X, Petrone N, Lee C H, Choi M S, Lee D Y, Lee C, Yoo W J, Watanabe K, Taniguchi T, Nuckolls C, Kim P and Hone J 2013 *ACS Nano* **7** 7931

[10] Biswas C and Lee Y H 2011 *Adv. Funct. Mater.* **21** 3806

[11] Eda G, Yamaguchi H, Voiry D, Fujita T, Chen M and Chhowalla M 2011 *Nano Lett.* **11** 5111

[12] Nair R R, Blake P, Grigorenko A N, Novoselov K S, Booth T J, Stauber T, Peres N M and Geim A K 2008 *Science* **320** 1308

[13] Meng J, Song H D , Li C Z , Jin Y, Tang L, Liu D, Liao Z M , Xiu F and Yu D P 2015 *Nanoscale* **7** 11611

[14] Zhang W, Chuu C P, Huang J K, Chen C H, Tsai M L, Chang Y H, Liang C T, Chen Y Z, Chueh Y L, He J H, Chou M Y and Li L J 2015 *Sci. Rep.* **4** 3826

[15] Roy K, Padmanabhan M, Goswami S, Sai T P, Ramalingam G, Raghavan S and Ghosh A 2013 *Nat. Nanotechnol.* **8** 826

[16] Xu H, Wu J, Feng Q, Mao N, Wang C and Zhang J 2014 *Small* **10** 2300

[17] Yasaei P, Fathizadeh A, Hantehzadeh R, Majee A K, El-Ghandour A, Estrada D, Foster C, Aksamija Z, Khalili-Araghi F and Salehi-Khojin A 2015 *Nano Lett.* **15** 4532

[18] Yu Q, Jauregui L A, Wu W, Colby R, Tian J, Su Z, Cao H, Liu Z, Pandey D, Wei D, Chung T F, Peng P, Guisinger N P, Stach E A, Bao J, Pei S S and Chen Y P 2011 *Nat. Mater.* **10** 443

[19] Malola S, Hakkinen H and Koskinen P 2010 *Phys. Rev. B* **81** 165447

[20] Kim K, Lee Z, Regan W, Kisielowski C, Crommie M F and Zettl A 2011 *ACS Nano* **5** 2142

[21] Lu J, Bao Y, Su C L and Loh K P 2013 *ACS Nano* **7** 8350

[22] Yazyev O V and Louie S G 2010 *Phys. Rev. B* **81** 195420

[23] Zhan L, Wan W, Zhu Z, Zhao Z, Zhang Z, Shih T M and Cai W 2017 *Nanotechnology* **28** 305601

[24] Zhu Z, Zhan L, Wan W, Zhao Z, Shih T M and Cai W 2017 *Nanoscale* **9** 14804

[25] Li X, Cai W, An J, Kim S, Nah J, Yang D, Piner R, Velamakanni A, Jung I, Tutuc E, Banerjee S K, Colombo L and Ruoff R S 2009 *Science* **324** 1312

[26] Zhao Z, Shan Z, Zhang C, Li Q, Tian B, Huang Z, Lin W, Chen X, Ji H, Zhang W and Cai W 2015 *Small* **11** 1418

[27] Li X, Wu J, Mao N, Zhang J, Lei Z, Liu Z and Xu H 2015 *Carbon* **92** 126

[28] Reina A, Son H B, Jiao L Y, Fan B, Dresselhaus M S, Liu Z F and Kong J 2008 *J. Phys. Chem. C* **112** 17741

[29] Ferrari A C, Meyer J C, Scardaci V, Casiraghi C, Lazzeri M, Mauri F, Piscanec S, Jiang D, Novoselov K S, Roth S and Geim A K 2006 *Phys. Rev. Lett.* **97** 187401

[30] Ago H, Kawahara K, Ogawa Y, Tanoue S, Bissett M A, Tsuji M, Sakaguchi H, Koch R J, Fromm F, Seyller T, Komatsu K and Tsukagoshi K 2013 *Appl. Phys. Express* **6** 075101

[31] Zhou K G, Withers F, Cao Y, Hu S, Yu G L and Casiraghi C 2014 *ACS Nano* **8** 9914

[32] Zhan Y, Liu Z, Najmaei S, Ajayan P M and Lou J 2012 *Small* **8** 966

[33] Wu S, Huang C, Aivazian G, Ross J S, Cobden D H and Xu X 2013 *ACS Nano* **7** 2768

[34] Lin Y F, Li W, Li S L, Xu Y, Aparecido-Ferreira A, Komatsu K, Sun H, Nakaharai S and Tsukagoshi K 2014 *Nanoscale* **6** 795

[35] Xu X, Gabor N M, Alden J S, Van Der Zande A M and Mceuen P L 2010 *Nano Lett.* **10** 562

[36] Gabor N M, Song J C W, Ma Q, Nair N L, Taychatanapat T, Watanabe K, Taniguchi T, Levitov L S and Jarillo-Herrero P 2011 *Science* **334** 648